IEEE Access
Multidisciplinary | Rapid Review | Open Access Journal

Received April 29, 2020, accepted May 17, 2020, date of publication May 25, 2020, date of current version June 4, 2020.

Digital Object Identifier 10.1109/ACCESS.2020.2997087

MTPA Control Strategy Based on Signal Injection for V/f Scalar-Controlled Surface Permanent Magnet Synchronous Machine Drives

KIBOK LEE[1], (Member, IEEE), AND YONGSU HAN[2], (Member, IEEE)
[1]Department of Mechatronics Engineering, Incheon National University, Incheon 22012, South Korea
[2]Power Conversion Research and Development Department, LG Electronics, Seoul 08592, South Korea

Corresponding author: Yongsu Han (yongsu.han17@gmail.com)

This work was supported by the National Research Foundation of Korea (NRF) under Grant NRF-2018R1C1B5085704.

ABSTRACT In this paper, a new maximum torque per ampere (MTPA) control method for surface permanent magnet synchronous motors (SPMSMs) controlled by the scalar control (*v/f*) method is proposed. The scalar control is a sensorless method that controls only the magnitude and the frequency of the stator voltage vector without the information of the rotor position. This method suggests the injection of the high frequency voltage signal in the stator current vector reference frame, which can be calculated from the measured phase currents, to avoid the use of rotor position information. In addition, this method adjusts only the magnitude of the stator voltage to minimize the stator current based on the calculated input power. Another merit of this method is the robustness of the MTPA control to machine parameter errors or variations. With this proposed method, the stator current can be minimized in the whole speed-torque range and the drive efficiency can be improved. Simulation and experimental results are provided to verify the performance of this control strategy.

INDEX TERMS V/f scalar control, maximum torque per ampere (MTPA), surface permanent magnet synchronous motor (SPMSM), high frequency voltage injection.

I. INTRODUCTION

Recently, energy saving is a crucial issue in many industrial applications. Permanent magnet synchronous motors (PMSMs) have replaced induction machines (IMs) since PMSMs offer higher power density and efficiency than IMs. In addition, the inverter-fed PMSM drives with both the vector and scalar control methods have significantly increased. The vector control method is superior to the scalar control method in terms of dynamic response, system efficiency, and so on. Nevertheless, the scalar control method is used in many applications that do not require high dynamic performance, such as fans or pumps, and it ensures a simple control design, a low-cost implementation, and an easier commissioning by the end user [1], [2]. In the scalar control, the constant flux control is used to minimize the no-load current and avoid the stator flux linkage saturation. However, this control results in the decrease of system efficiency because of the excessive stator current under load conditions.

The associate editor coordinating the review of this manuscript and approving it for publication was Sing Kiong Nguang.

In this study, we propose a MTPA control method that can enhance the efficiency of SPMSMs controlled by the *v/f* scalar control method by minimizing the stator current. This method applies for the scalar-controlled drives that do not require the information of the rotor position.

The MTPA control methods for scalar-controlled PMSMs have been proposed in [2]–[9]. In [2]–[5], the MTPA control methods were implemented with two control loops to correct the stator voltage amplitude and phase by regulating the reactive power. These methods could achieve the fast dynamic response and high efficiency. However, intensive calculations and accurate information of machine parameters were required. Thus, if the motor parameters such as stator inductance vary with temperature and flux saturation, the MTPA control cannot be guaranteed. The approach in [6]–[8] proposed the voltage amplitude correction method based on the power-factor angle error. The power-factor angle reference for the MTPA operation is calculated with machine parameters considering the operating condition. However, the algorithm in this method is complicated and is sensitive to the parameter errors. Method described in [9] proposes

the use of the d-axis current error to implement the MTPA control. This method has good control performances over wide operating speed ranges. However, because it requires the information of the rotor position, it is not suitable for the v/f-controlled drives. The major advantages of the v/f control is that it does not require the rotor position information.

In [10]–[13], the MTPA control methods were introduced for vector controlled PMSMs. In [10], the high frequency signal is injected into the flux reference. The torque variation caused by the current vector angle becomes zero at the MTPA points, and thus the MTPA points can be tracked. However, the measurement of the torque variation is difficult. In [11], the high frequency current signal is injected and the speed variation instead of the torque variation is used to track MTPA points. The performance of this method is limited by the resolution of the speed/position sensor. In [12], the high frequency current signal is injected and the input power is used to track the MTPA points. This current signal injection method requires the rotor position information and two high-frequency current regulators. In [13], a method was proposed to inject the virtual current signal to track the MTPA points. This method avoids additional loss by the injected signal. However, similar to other approaches in [10]–[12], this method also requires the rotor position information, which is unknown in the scalar control method. Consequently, these methods cannot be applied to achieve the MTPA control for scalar-controlled SPMSM drives.

We propose a new MTPA control method suitable for scalar-controlled SPMSM drives. This method injects the high frequency voltage signal to track the MTPA operating points and does not use the rotor position information. The remainder of this paper illustrates the principles of the proposed MTPA control method. We also verify the performance of this method using simulation and experimental results.

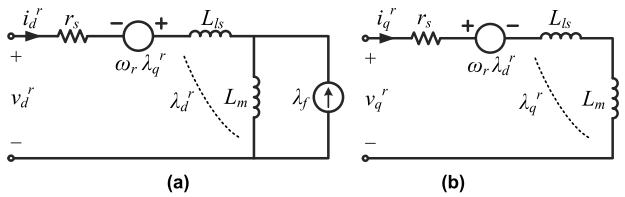

FIGURE 1. Equivalent circuit of the SPMSM in the rotor reference frame; (a) d-axis circuit (b) q-axis circuit.

II. CONVENTIONAL SCALAR CONTROL METHOD

The machine equivalent circuit is shown in Fig. 1. The SPMSM machine equation can be described in the rotor reference frame [2], [3], as follows:

$$\begin{bmatrix} v_d^r \\ v_q^r \end{bmatrix} = \begin{bmatrix} r_s + pL_s & -\omega_r L_s \\ \omega_r L_s & r_s + pL_s \end{bmatrix} \begin{bmatrix} i_d^r \\ i_q^r \end{bmatrix} + \begin{bmatrix} 0 \\ \omega_r \lambda_f \end{bmatrix} \quad (1)$$

where p is the derivative operator, r_s is the stator winding resistance, L_s is the stator inductance, v_d^r and v_q^r are the d-q axis stator voltages in the rotor reference frame, i_d^r and i_q^r are the d-q axis stator currents in the rotor reference frame, and ω_r and λ_f are the electrical angular frequency of the rotor and the permanent magnet (PM) flux linkage, respectively. In the vector control methods, the quantities in the stator reference frame are transformed into the rotor reference frame to remove the dependency on the rotor position, where the d-axis is aligned with the electrical position of the rotor flux. Therefore, the vector control methods need the speed and position sensors such as the encoder and resolver. This increases the system cost and reduce the system reliability. Alternatively, the sensorless control can be used to estimate the rotor position and speed by using model-based observers or the high frequency signal injection. However, the sensorless control increases the complexity of the control, and the system performance is degraded by the errors of machine parameters.

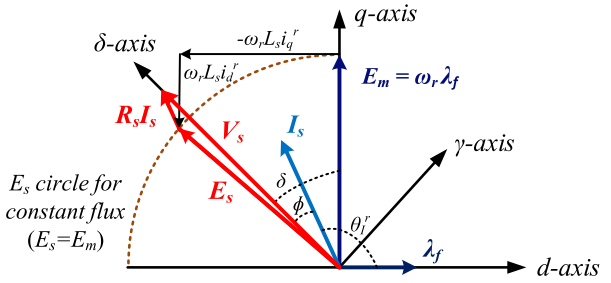

FIGURE 2. Phasor diagram of constant stator flux v/f controlled SPMSM in a steady state.

In the v/f control method, the amplitude and the frequency of the voltage vector are only controlled without the rotor position information. The γ-δ axis synchronous reference frame is generally used for the control, where the δ-axis is aligned with the stator voltage vector. The v/f control method can be easily implemented compared to the vector control methods. Fig. 2 shows the phasor diagram of the stator voltage and current vectors in the γ-δ and d-q synchronous reference frames. The δ-axis and d-axis are aligned with the stator voltage vector and the rotor flux direction, respectively. The equation of the SPMSM machine in the γ-δ axis reference frame can be written as

$$\begin{bmatrix} v_\gamma^e \\ v_\delta^e \end{bmatrix} = \begin{bmatrix} r_s + pL_s & -\omega_e L_s \\ \omega_e L_s & r_s + pL_s \end{bmatrix} \begin{bmatrix} i_\gamma^e \\ i_\delta^e \end{bmatrix} + \omega_e \lambda_f \begin{bmatrix} \sin\delta \\ \cos\delta \end{bmatrix} \quad (2)$$

where v_γ^e and v_δ^e are the γ-axis and δ-axis voltages, and i_γ^e and i_δ^e are the γ-axis and δ-axis currents, respectively. ω_e is the synchronous angular frequency of the voltage vector and δ is the load angle.

The v/f control for the PMSMs is inherently unstable because of the nonexistence of the damper winding unlike that for the IMs [9], [14]. Hence, under significant load disturbance, the v/f controlled PMSMs easily lose synchronization. In general, the v/f control method for synchronous motors requires the stabilizing loop to ensure the stable operation in all operating ranges. Fig. 3 shows the conventional v/f control method with the stabilizing loop [14]. To tolerate the external disturbance, the synchronous frequency ω_e is calculated with the speed command ω_0 and the frequency modulation signal $\Delta\omega_e$. The frequency modulation signal is generated in the

stabilizing loop based on the input power calculated with the voltage commands and the stator currents. The calculated input power is passed through the high-pass filter to extract the power perturbation. Then, the frequency modulation signal $\Delta\omega_e$ is obtained by multiplying the proportional gain k_p with the power perturbation. The gain k_p is properly selected to place the system poles in the stable region [14].

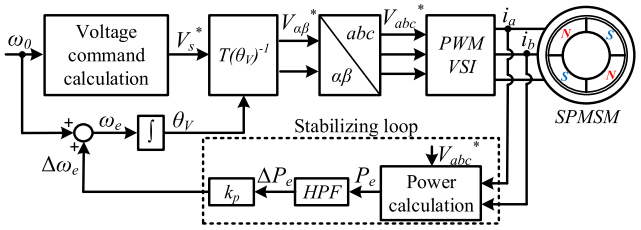

FIGURE 3. Conventional scalar control with the stabilizing loop.

The magnitude of the voltage command is calculated to maintain a constant stator flux linkage and it can be instantaneously calculated with the speed command ω_0 and the permanent magnet flux linkage λ_f as

$$V_s^* = \omega_0 \lambda_f. \tag{3}$$

Furthermore, considering the stator resistance voltage drop, the stator voltage command in (3) is rewritten as [14]

$$V_s^* = r_s I_s \cos\phi + \sqrt{\left(\omega_0 \lambda_f\right)^2 - \left(r_s I_s \sin\phi\right)^2} \tag{4}$$

where I_s is the magnitude of the current vector, and ϕ is the power factor angle. With this selection, the magnitude of E_s in Fig. 2 satisfies the equation below in all operating conditions.

$$|E_s| = |E_m| = \omega_0 \lambda_f \tag{5}$$

where E_s and E_m are the voltage vectors induced by the stator flux linkage and the permanent magnet flux linkage, respectively. Then, the machine has the same torque capability in all operating ranges, and the no-load current is minimized as keeping comparably the low stator voltage [14]. However, it is difficult to certify the minimum current at the no-load condition in case of varying motor parameters such as the stator resistance and the permanent magnet flux linkage. Furthermore, if the load and the stator current increase as the machine speed is constant, the negative d-axis current is required to satisfy the voltage condition of (5), as shown in Fig. 2. This reduces the efficiency of SPMSM as a result of increased copper loss [12].

Fig. 4 shows the phasor diagram of the stator voltage and current vectors in the case of the MTPA control. Although the load torque varies, the d-axis current maintains zero value as the magnitude of E_s varies. Fig. 5 shows simulation results of the d-q axis stator currents when the SPMSM is operated with the v/f constant stator flux control and the MTPA control. The rotor speed in this simulation is fixed at a rated speed of 1,500 [r/min] and the load torque is increased from 0 [N · m] to the full load, that is, 16 [N · m].

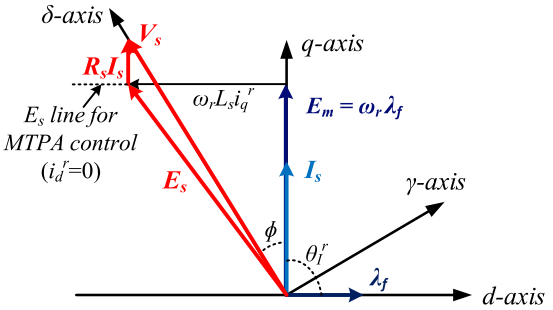

FIGURE 4. Phasor diagram of MTPA control for SPMSM in a steady state.

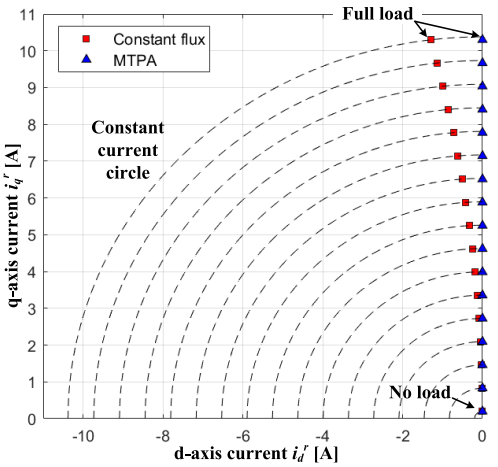

FIGURE 5. d-q axis current in the current plane under the constant stator flux linkage control (v/f) and the MTPA control for SPMSM.

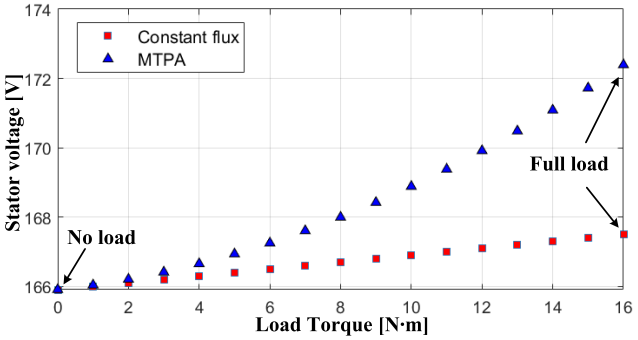

FIGURE 6. Stator voltage magnitude at different load torque and the fixed speed 1,500 [r/min] conditions under the constant stator flux linkage control (v/f) and the MTPA control.

The machine parameters are listed in Table 1. The red dots represent the d-q axis currents under the constant stator flux linkage control, which is the conventional v/f control method. As the load torque increases, the magnitude of negative d-axis current gradually increases, resulting in a decrease in the motor efficiency [12]. The blue dots represent the d-q axis currents with the MTPA control. The d-axis current remains zero as the load torque increases, and the magnitude of the stator current with the MTPA control is less than that with the constant flux linkage control. Fig. 6 shows the simulation results of the stator voltage magnitudes with the same conditions as in Fig. 5. The red and blue dots represent the stator

TABLE 1. Test SPMSM parameters.

Parameter	Unit	Symbol	Values
Rated Power	[kW]	P_{out}	3.0
Rated Speed	[rpm]	N_r	1750
Rated Torque	[N·m]	T_e	16
Rated Voltage (line-line)	[Vrms]	V_s	220
Phase Current	[Arms]	i_s	7.8
Pole	-	P	8
Stator Resistance	[Ω]	r_s	0.158
Stator Inductance	[mH]	L_s	6.3
Flux Linkage	[V·s]	λ_f	0.264
Inertia	[N·m/(rad·s^{-2})]	J	0.01
Switching Frequency	[kHz]	f_{sw}	10
Inverter DC-link Voltage	[V]	$V_{DC\text{-}link}$	310

voltage magnitudes with the constant stator flux control and the MTPA control, respectively. The simulation results show that the MTPA control can be achieved by adjusting the stator voltage magnitude in the *v/f* controlled drives.

In this study, we propose the adjustment of the stator voltage magnitude to achieve the MTPA control for *v/f* scalar controlled SPMSM drives, which can maintain the minimum stator current at all operating conditions.

III. PROPOSED MTPA METHOD FOR SCALAR-CONTROLLED SPMSM DRIVES

As a well-known theoretical basis, the electromagnetic torque generated by an SPMSM is given as follows [15].

$$T_e = \frac{3}{2}\frac{P}{2}\lambda_f i_q^r \tag{6}$$

where P is the pole number of the rotor. The generated torque is only proportional to the q-axis stator current because there is no saliency in the rotor of the SPMSM. Thus, the MTPA operation can be achieved at a zero d-axis stator current. In the vector control method, the d-q axis stator currents are directly controlled using the d-q axis current regulators as well as by knowing the rotor position through the speed and position sensor or the sensorless algorithm. However, the rotor position is not known in the *v/f* control method. Hence, an alternative method that does not need the information of the rotor position for implementing the MTPA control is required.

A. BASIC CONCEPT OF THE PROPOSED METHOD

Fig. 7 shows the torque variation by the current vector angle perturbation at different operating points. When the MTPA control is implemented, the current vector is aligned with the q-axis in the rotor reference frame and the torque variation by the current vector angle perturbation is always zero as shown in Fig. 7. The differentiation of the electric torque with respect to the current angle is written as

$$\left.\frac{\partial T_e}{\partial \theta}\right|_{\theta_{MTPA}} = \frac{3P}{4}\lambda_f I_s \cos\theta_{MTPA} = 0 \tag{7}$$

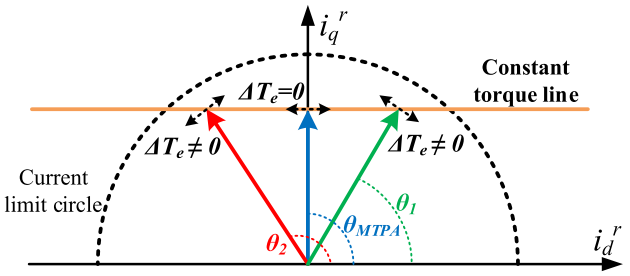

FIGURE 7. Constant torque by stator current in the current plane, and the torque variation caused by the current vector angle perturbation.

where θ_{MTPA}, which is $\pi/2$ [rad], is the MTPA angle for the SPMSM in the rotor reference frame. The basic concept of this proposed method is tracking the point where the differential of the torque becomes zero while regulating the stator voltage magnitude. Then, the MTPA control can be implemented without the information of the rotor position angle in the *v/f* control method.

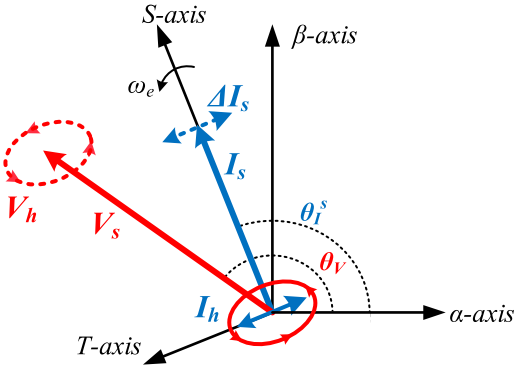

FIGURE 8. Phasor diagram of the injected high frequency voltage and the induced current in the S-T axis synchronous reference frame.

B. HIGH FREQUENCY VOLTAGE INJECTION

To find the MTPA angle θ_{MTPA} that satisfies (7), high frequency voltage is injected to generate the perturbation of the current vector angle. Fig. 8 shows the phasor diagram of the injected voltage and the induced current in the S-T axis current vector synchronous reference frame, where the S-axis is aligned with the stator current vector. The high frequency voltage equation of the SPMSM in the S-T axis reference frame can be written as follows [12], [16]–[18].

$$\begin{bmatrix} v_{Sh}^e \\ v_{Th}^e \end{bmatrix} = \begin{bmatrix} r_{sh}+pL_{sh} & -\omega_e L_{sh} \\ \omega_e L_{sh} & r_{sh}+pL_{sh} \end{bmatrix} \begin{bmatrix} i_{Sh}^e \\ i_{Th}^e \end{bmatrix} \tag{8}$$

where v_{Sh}^e, v_{Th}^e, and i_{Sh}^e, i_{Th}^e are the high frequency components of the stator voltage and the stator current. r_{sh} and L_{sh} are the stator resistance and inductance at the injected high frequency, respectively. Assuming that the injected voltage frequency is sufficiently high, the reactance is significantly larger than the resistance, and for simplification, we consider the resistance voltage drop terms to be negligible. However, the decoupling term cannot be neglected because of the high speed condition that ω_e is close to the injected voltage frequency ω_h. Then, the voltage equation (8) can be simplified

and expressed with ω_h in a steady state as

$$\begin{bmatrix} v_{Sh}^e \\ v_{Th}^e \end{bmatrix} = \begin{bmatrix} j\omega_h L_{sh} & -\omega_e L_{sh} \\ \omega_e L_{sh} & j\omega_h L_{sh} \end{bmatrix} \begin{bmatrix} i_{Sh}^e \\ i_{Th}^e \end{bmatrix}. \quad (9)$$

This method aims to generate the high frequency current I_h orthogonal to the current vector I_s as shown in Figs. 7 and 8. To generate only the T-axis high frequency current component, the injected high frequency voltage commands can be calculated as

$$\begin{aligned} v_{Sh}^{e*} &= -\omega_0 L_{sh} \Delta I_s \sin \omega_h t \\ v_{Th}^{e*} &= \omega_h L_{sh} \Delta I_s \cos \omega_h t \end{aligned} \quad (10)$$

where ΔI_s is the expected amplitude of the induced high frequency current I_h. In this study, we fix ΔI_s to be 0.2 [A], considering the rated current of the machine, the amplitude of the high frequency voltage, the additional copper loss, and the oscillation torque by the injected voltage. By injecting the high frequency voltages of (10), the high frequency current can be generated only in the T-axis, and then the resulting S-T axis currents are expressed as

$$\begin{aligned} i_S^e &= I_S^e + i_{Sh}^e = I_s \\ i_T^e &= I_T^e + i_{Th}^e = \Delta I_s \sin \omega_h t. \end{aligned} \quad (11)$$

Here, the current vector I_s in the S-axis is generated by the voltage vector V_s, and the high frequency current $\Delta I_s sin\ \omega_h t$ in the T-axis is induced by the high frequency voltage V_h as in Fig. 8.

The inverter system requires the voltage commands in the stationary reference frame. Therefore, the S-T axis synchronous reference frame of (10) is transformed to the α-β axis stationary reference frame, as follows:

$$\begin{aligned} v_{\alpha h}^* &= -\omega_0 L_{sh} \Delta I_s \sin \omega_h t \cos \theta_I^s - \omega_h L_{sh} \Delta I_s \cos \omega_h t \sin \theta_I^s \\ v_{\beta h}^* &= -\omega_0 L_{sh} \Delta I_s \sin \omega_h t \sin \theta_I^s + \omega_h L_{sh} \Delta I_s \cos \omega_h t \cos \theta_I^s \end{aligned} \quad (12)$$

where $v_{\alpha h}^*$, $v_{\beta h}^*$, and θ_I^s are the high frequency voltage commands and the current vector angle in the stationary reference frame, respectively. This transformation requires the current vector angle in the stationary reference frame.

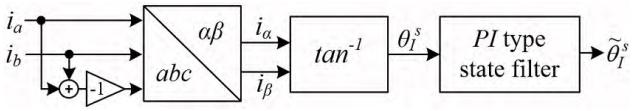

FIGURE 9. Filtered angle estimation of the current vector in the stationary reference frame.

Fig. 9 shows the block diagram to calculate the current vector angle θ_I^s. The current vector angle can be calculated using two-phase stator currents measured with the current sensors. However, the injected high frequency voltage from (12) and the frequency modulation signal of the stabilizing loop in Fig. 3 cause current vector phase oscillation. To track the correct MTPA angle θ_{MTPA} as in Fig. 7, the high frequency voltages should be injected in the current vector reference frame after the oscillation term is eliminated. The PI-type state filter is used to filter out the current vector phase oscillation. The transfer function of the state filter is described by

$$\frac{\tilde{\theta}_I^s}{\theta_I^s} = \frac{K_P s + K_I}{s^2 + K_P s + K_I}. \quad (13)$$

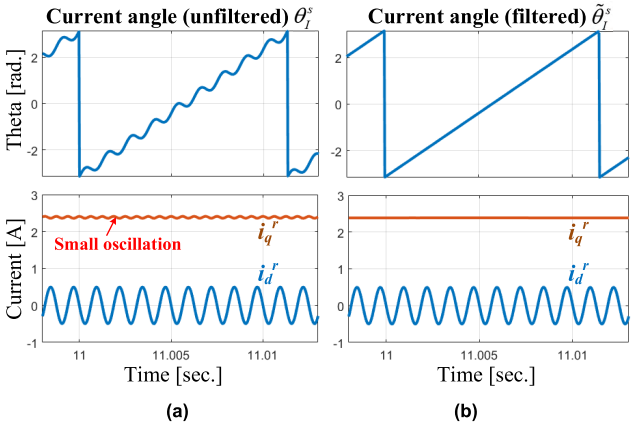

FIGURE 10. Current vector angle in the stationary reference frame and the d-q axis current in the rotor reference frame using (a) the unfiltered current vector angle and (b) the filtered current vector angle.

The PI gains are set to place all closed-loop eigenvalues at 100 [rad/s], which is considerably lower than the injected voltage frequency. Figs. 10(a) and (b) show each of the simulation results when the unfiltered current angle θ_I^s and the filtered current angle $\tilde{\theta}_I^s$ are used in (12). In this simulation, the injected voltage frequency is set to 800 [Hz] and the amplitude of the induced high frequency current is set to 0.5 [A]. This is to clearly show the difference between the two conditions. The machine parameters listed in Table 1 are used and the machine is controlled to operate at the MTPA point. In Fig. 10(a), when the unfiltered current vector angle θ_I^s is used, the q-axis current includes the small oscillation component. This is not the desired result because the high frequency current is not orthogonal to the q-axis. By contrast, in Fig. 10(b), the filtered current vector angle $\tilde{\theta}_I^s$ is used, so the high frequency current is only induced in the d-axis current. Then, the high frequency current is orthogonal to the current vector I_s as shown in Fig. 7. Fig. 11 shows the block diagram for calculating the high frequency voltage commands in the stationary reference frame. It requires only the filtered current vector angle and stator inductance and not the rotor position information.

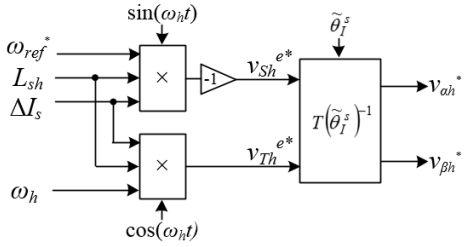

FIGURE 11. Calculation of the high frequency voltage command in the stationary reference frame.

C. STATOR VOLTAGE ADJUSTMENT FOR MTPA OPERATION

This MTPA method adjusts only the stator voltage magnitude based on the processed input power while injecting high-frequency voltage. This section describes the procedure for obtaining the processed input power and the relationship between the processed input power and the MTPA angle.

The electric input power consists of the copper loss, reactive power, and mechanical power [12]. The copper loss occurs in stator winding, and it is expressed in terms of the stator resistance and stator current as follows:

$$P_{copper} = \frac{3}{2} r_s I_s^2. \tag{14}$$

To consider the effect of the injected high-frequency signal, the copper loss can be rewritten with the *S-T* axis currents by substituting (11) into (14); thus:

$$\begin{aligned} P_{copper} &= \frac{3}{2} r_s \left(i_S^{e2} + i_T^{e2} \right) \\ &= \frac{3}{2} r_s \left(I_s^2 + \frac{1}{2} \Delta I_s^2 - \frac{\Delta I_s^2}{2} \cos 2\omega_h t \right). \end{aligned} \tag{15}$$

The copper loss consists of two *DC* components and the high-frequency component, which is twice as high as the injected voltage frequency. The additional copper loss caused by the high frequency current can be neglected because ΔI_s is small enough [12].

Similarly, the reactive power can be expressed with the *S-T* axis currents as

$$P_{reactive} = \frac{3}{2} L_s \left(\frac{di_S^e}{dt} i_S^e + \frac{di_T^e}{dt} i_T^e \right) = \frac{3}{4} L_s \omega_h \Delta I_s^2 \sin 2\omega_h t. \tag{16}$$

The frequency of the reactive power is twice faster than one of the injected voltage.

The last term of the electrical input power is the mechanical power proportional to the q-axis current as derived in (6) and it can be expressed as:

$$\begin{aligned} P_{mech} &= \frac{3}{2} \omega_r \lambda_f i_q^r = \frac{3}{2} \omega_r \lambda_f \left(i_S^e \sin\theta_I^r + i_T^e \cos\theta_I^r \right) \\ &= \frac{3}{2} \omega_r \lambda_f \left(I_s \sin\theta_I^r + \Delta I_s \cos\theta_I^r \sin\omega_h t \right) \end{aligned} \tag{17}$$

where θ_I^r is the current vector angle in the synchronous rotor reference frame. The proposed method does not use this angle, which can be calculated with the rotor position information, for implementing the MTPA control. It is only introduced to show how the MTPA point can be estimated using the input power. The mechanical power P_{mech} consists of the *DC* and *AC* components. Notably, the mechanical power includes the current vector angle information θ_I^r and the frequency of the *AC* component is the same as one of the high frequency voltage. When the machine operates at the MTPA point, the current vector angle θ_I^r is $\pi/2$ [rad.] and the *AC* component becomes zero. From this result, the MTPA control can be implemented by regulating the *AC* component extracted from (17). In addition, the torque oscillation caused by the injected voltage becomes zero when the MTPA control is achieved.

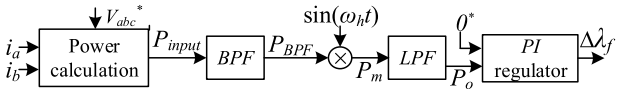

FIGURE 12. Signal processing of the input power, and the flux linkage constant adjustment for MTPA operation.

Fig. 12 shows the signal process to extract only the *AC* component of (17). First, passing the input power P_{input} through the band-pass filter (BPF), whose center frequency is set to the injected frequency ω_h, the other frequency components in (15), (16), and (17) are filtered out and the following component is extracted as follows:

$$P_{BPF} = \frac{3}{2} \omega_r \lambda_f \Delta I_s \cos\theta_I^r \sin\omega_h t. \tag{18}$$

Next, P_{BPF} is multiplied with the injected high frequency signal. The modulated input power P_m is obtained and it consists of the *DC* term and the oscillation term as follows.

$$P_m = \frac{3}{4} \omega_r \lambda_f \Delta I_s \cos\theta_I^r - \frac{3}{4} \omega_r \lambda_f \Delta I_s \cos\theta_I^r \cos 2\omega_h t. \tag{19}$$

P_m passes through the low-pass filter (LPF) to filter out the second term of (19). The cutoff frequency of the LPF is chosen to be considerably lower than the injected signal frequency ω_h. The resultant input power is expressed as

$$P_o = \frac{3}{4} \omega_r \lambda_f \Delta I_s \cos\theta_I^r. \tag{20}$$

When the current vector angle θ_I^r is $\pi/2$ [rad.], the resultant input power P_o becomes zero. In other words, by controlling the resultant input power to be zero, the current vector can be aligned with the q-axis in the rotor reference frame and the MTPA operation for SPMSM can be implemented in the *v/f* control without the information on the rotor position angle. The PI regulator in Fig. 12 is used to make the resultant input power P_o be zero. The output of the PI regulator is the compensation term $\Delta\lambda_f$ used to adjust the voltage command. This work adjusts the flux linkage constant λ_f instead of the stator voltage command V_s^* because it results in the convergence time to the MTPA points being less sensitive to the operating speed and torque conditions. The stator voltage command from (3) is modified to include the compensation term $\Delta\lambda_f$ generated from the PI regulator as follows:

$$V_s^* = \omega_0 \left(\lambda_f + \Delta\lambda_f \right) = \omega_0 \lambda_f^* \tag{21}$$

where λ_f^* is the flux reference.

Fig. 13 shows the proposed complete drive scheme for the MTPA control of the SPMSM controlled by the *v/f* control method. The dotted block indicates the proposed method.

D. PARAMETER SENSITIVITY

While implementing the proposed MTPA control method, the stator resistance, the stator inductance, and the permanent magnet flux linkage can be varied by factors such as stator current and temperature [2], [13], [19]–[22]. Therefore,

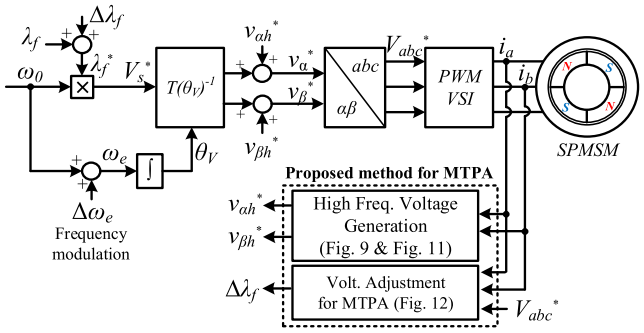

FIGURE 13. Complete drive scheme with the proposed MTPA control strategy.

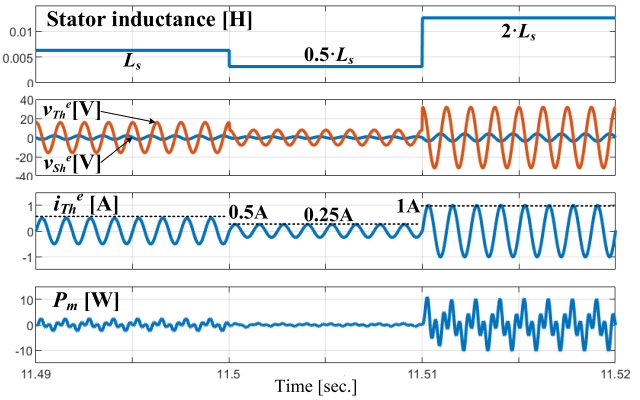

FIGURE 14. Simulation result for the parameter sensitivity check in case the high frequency voltage command has the stator inductance error.

the effects of the machine parameter errors are analyzed in this section.

First, the resistance voltage drop term in (8) can be neglected because the reactance is considerably larger than the resistance in terms of high-frequency components. Therefore, the high frequency voltage commands from (10) and the induced high-frequency currents from (11) are not affected by the stator resistance error. In addition, the stator resistance value is not used in this proposed method as shown in Fig. 13.

Next, the effect of the stator inductance error is analyzed. Equation (9) can be rewritten in the form of a differential equation for the S-T axis high-frequency currents as follows.

$$p\begin{bmatrix} i^e_{Sh} \\ i^e_{Th} \end{bmatrix} = \begin{bmatrix} 0 & \omega_e \\ -\omega_e & 0 \end{bmatrix}\begin{bmatrix} i^e_{Sh} \\ i^e_{Th} \end{bmatrix} + \frac{1}{L_{sh}}\begin{bmatrix} v^{e*}_{Sh} \\ v^{e*}_{Th} \end{bmatrix}. \quad (22)$$

Here, the high frequency voltage commands can be determined from (10), with the inductance error as in the following equations:

$$\begin{aligned} v^{e*}_{Sh} &= -\omega_0 \left(L_{sh} + \Delta L_{sh}\right) \Delta I_s \sin \omega_h t \\ v^{e*}_{Th} &= \omega_h \left(L_{sh} + \Delta L_{sh}\right) \Delta I_s \cos \omega_h t \end{aligned} \quad (23)$$

where ΔL_{sh} is the stator inductance error. By substituting (23) into (22), the resulted high frequency currents become

$$\begin{aligned} i^e_{Sh} &= 0 \\ i^e_{Th} &= \left(1 + \frac{\Delta L_{sh}}{L_{sh}}\right) \Delta I_s \sin \omega_h t. \end{aligned} \quad (24)$$

From (11) and (24), the stator inductance error affects only the amplitude of the induced high frequency current. Fig. 14 shows the simulation result when the high frequency voltage command has the stator inductance error. The rotor speed in this simulation is fixed at 1,500 [r/min], the amplitude of the induced high frequency current is set to be 0.5 [A], and the machine is controlled to operate at the MTPA point. In this simulation, the stator inductance is intentionally varied from 1 p.u. via 0.5 p.u. to 2 p.u. to observe the parameter sensitivity of the proposed method. As expected from (24), the amplitude of the high frequency current is proportionally varied with respect to the stator inductance error. The amplitude of the modulated input power P_m is also proportionally varied, but maintaining an average value of zero. From (19), the zero average value of P_m indicates that the current vector angle θ^r_I is $\pi/2$ [rad]. This simulation result verifies that the performance of the proposed MTPA control is not affected by the stator inductance error.

Finally, the permanent magnet flux linkage is used to calculate the voltage command in this v/f scalar control. From (21), the permanent magnet flux linkage λ_f is adjusted with the compensation term $\Delta\lambda_f$ to achieve the MTPA control. Therefore, the permanent magnet flux error or variation only affects the value of $\Delta\lambda_f$ and does not affect the steady-state performance of this MTPA control. As a result, the proposed method ensures the MTPA tracking performance even if the machine parameters have errors.

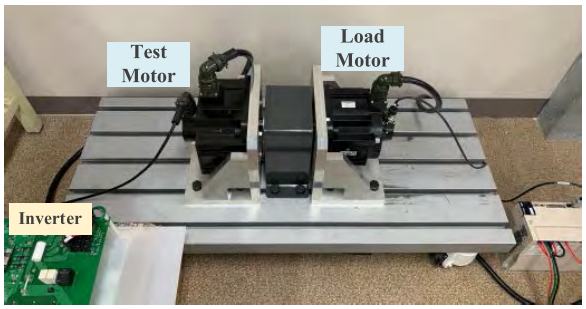

FIGURE 15. Dynamo set configuration for the experimental test.

IV. EXPERIMENTAL RESULTS

The experimental verification of the proposed MTPA control was conducted on a 3 kW SPMSM, whose parameters are listed in Table 1. Fig. 15 shows the photograph of the experimental set, where a servo motor is coupled to the test motor as a load machine, and an encoder is used to monitor solely the d-axis current to validate the MTPA operation. The high frequency voltage commands were determined from (10) to achieve an induced current of 0.2 [A]. The frequency of the injected signal was chosen to be 800 [Hz], with consideration of the switching frequency and voltage margin of the inverter.

As shown in Figs. 16(a) and (b), the flux reference λ^*_f from (21) was varied manually within the range of the optimal value for the MTPA operation, at a fixed rotor speed of 1,500 [r/min]. In Fig. 16(a), a half-load condition of

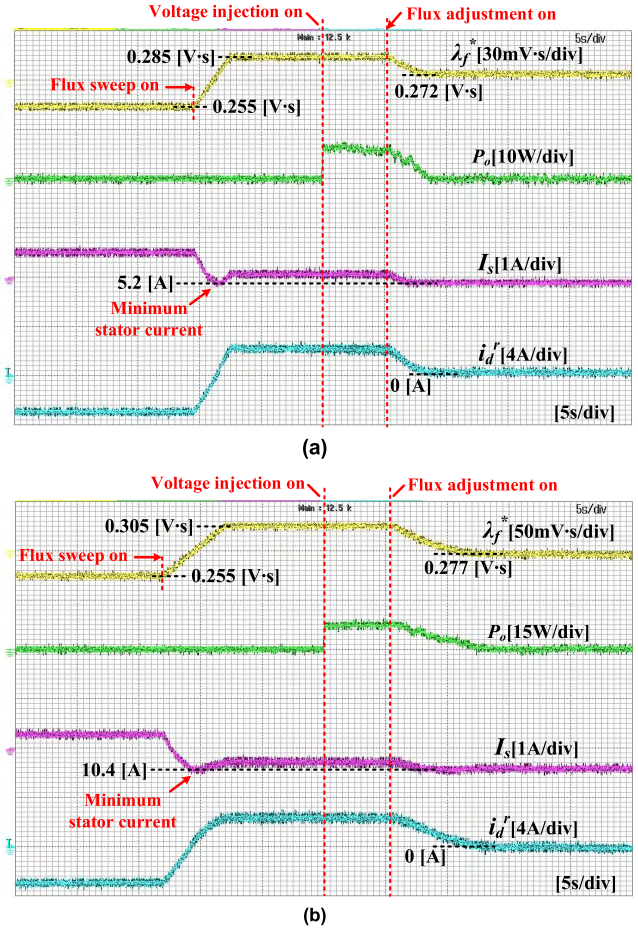

FIGURE 16. Experimental results: the flux reference (yellow line), the resultant input power (green line) for tracking MTPA points, the phase current magnitude (violet line), and the d-axis current (cyan line) at (a) 1,500 [r/min], half-load condition of 8 [N · m] and (b) 1,500 [r/min], full-load condition of 16 [N · m].

approximately 8 [N · m] was applied to the machine and the flux reference sweep was performed within the left-half region of the plot.

In the right-half region of the plot, the proposed method started tracking the MTPA point. First, the high frequency voltage was injected to generate the resultant input power P_o. After the flux adjustment control was enabled, the operating point moved to the MTPA point by the flux reference adjustment term generated from the PI regulator shown in Fig. 12. The MTPA operation can be confirmed by the minimized phase current magnitude (violet line) and the zero d-axis current (cyan line). Fig. 16(b) shows the experimental result at a full-load condition of approximately 16 [N · m]. In this experiment, the optimal flux reference value was different from that of Fig. 16(a). The phase current was minimized and the d-axis current became zero after the proposed MTPA control was enabled.

Fig. 17 shows the MTPA tracking performance with varying load torque. In the left-half region of the plot, the flux reference (green line) was fixed to the value listed in Table 1 and the load torque (yellow line) was varied from

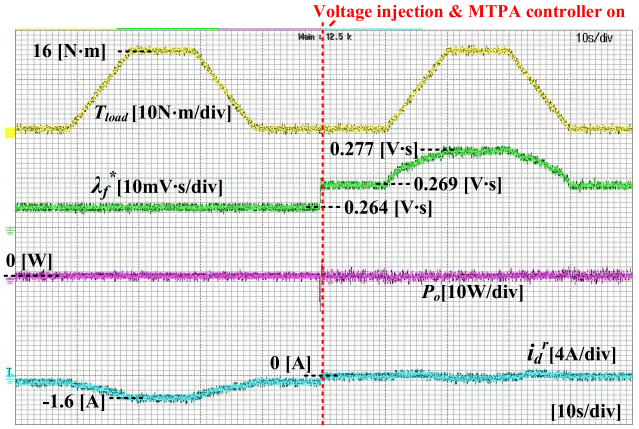

FIGURE 17. Experimental results: the load torque (yellow line), flux reference (green line), resultant power (violet line) for tracking MTPA points, and d-axis current (cyan line) at 1,500 [r/min].

0 [N · m] to 16 [N · m]. The rotor speed was fixed at 1,500 [r/min]. The d-axis current showed a negative value in the whole load range, and it gradually increased as the load torque increased. This d-axis current does not contribute to the electric torque but only causes additional copper loss in the stator windings. In the right-half region of the plot, the proposed method was applied and the flux reference was adjusted on the basis of the resultant input power obtained from the voltage injection and the signal processing. The flux reference (green line) was adjusted as the load torque varied. Consequently, the d-axis current remained almost zero. As a result, this proposed method could achieve the MTPA operation in the whole load range by adjusting the flux reference.

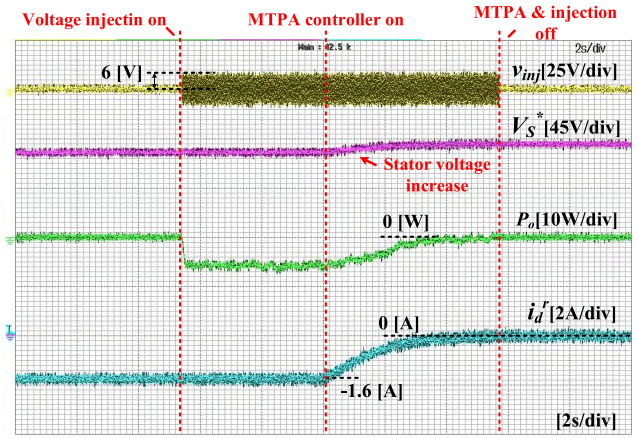

FIGURE 18. Experimental results: the high frequency injection voltage (yellow line), stator command voltage (green line), resultant power (violet line) for tracking MTPA points, and d-axis current (cyan line) at 1,500 [r/min].

The experimental result in Fig. 18 verifies that the proposed method can maintain the MTPA operation with the adjusted magnitude of the stator voltage command even after the high frequency injection and the MTPA controller are disabled. Therefore, this method suggests enabling the MTPA tracking algorithm for several seconds periodically or after

when the speed command is changed or the magnitude of the stator current is considerably varied. This experimental result also shows that the amplitude of high frequency voltage to induce a high-frequency current of 0.2 [A] was approximately 6 [V] at the rated speed, which corresponds to the worst case.

V. CONCLUSION

This study proposed a new MTPA control method that is applicable for *v/f* scalar-controlled SPMSMs. The lack of knowledge of the rotor position is one of the most challenging problems in the scalar control method. This method can successfully track the MTPA operating points and minimize the stator current without the information of the rotor position. This method injects high-frequency voltage in the current vector frame, which is calculated from the measured phase currents, instead of the rotor reference frame. In addition, only the magnitude of the stator voltage is regulated to achieve the MTPA control based on the calculated input power. Finally, the robustness to the machine parameters was analyzed and the performance of the proposed MTPA method for scalar-controlled SPMSMs was verified using simulation and experimental results.

REFERENCES

[1] M. Štulrajter, V. Hrabovcová, and M. Franko, "Permanent magnets synchronous motor control theory," *J. Electr. Eng., Slovak Republic*, vol. 58, no. 2, pp. 79–84, 2007.
[2] J.-I. Itoh, N. Nomura, and H. Ohsawa, "A comparison between V/f control and position-sensorless vector control for the permanent magnet synchronous motor," in *Proc. Power Convers. Conf.*, vol. 3, Apr. 2002, pp. 1310–1315.
[3] R. Ancuti, I. Boldea, and G.-D. Andreescu, "Sensorless V/f control of high-speed surface permanent magnet synchronous motor drives with two novel stabilising loops for fast dynamics and robustness," *IET Electr. Power Appl.*, vol. 4, pp. 149–157, Mar. 2010.
[4] J.-I. Itoh, Y. Nakajima, and M. Kato, "Maximum torque per ampere control method for IPM synchronous motor based on V/f control," in *Proc. IEEE 10th Int. Conf. Power Electron. Drive Syst. (PEDS)*, Apr. 2013, pp. 1322–1327.
[5] S.-M. Sue, T.-W. Hung, J.-H. Liaw, Y.-F. Li, and C.-Y. Sun, "A new MTPA control strategy for sensorless V/f controlled PMSM drives," in *Proc. 6th IEEE Conf. Ind. Electron. Appl. (ICIEA)*, Beijing, China, Jun. 2011, pp. 1840–1844.
[6] A. Consoli, G. Scelba, G. Scarcella, and M. Cacciato, "An effective energy-saving scalar control for industrial IPMSM drives," *IEEE Trans. Ind. Electron.*, vol. 60, no. 9, pp. 3658–3669, Sep. 2013.
[7] S.-C. Agarlita, G.-D. Andreescu, C.-E. Coman, and I. Boldea, "Stable V/f control system with controlled power factor angle for permanent magnet synchronous motor drives," *IET Electr. Power Appl.*, vol. 7, no. 4, pp. 278–286, Apr. 2013.
[8] Y. Nakamura, T. Kudo, F. Ishibashi, and S. Hibino, "High-efficiency drive due to power factor control of a permanent magnet synchronous motor," *IEEE Trans. Power Electron.*, vol. 10, no. 2, pp. 247–253, Mar. 1995.
[9] Z. Tang, X. Li, S. Dusmez, and B. Akin, "A new V/f-based sensorless MTPA control for IPMSM drives," *IEEE Trans. Power Electron.*, vol. 31, no. 6, pp. 4400–4415, Jun. 2016.
[10] S. Bolognani, L. Peretti, and M. Zigliotto, "Online MTPA control strategy for DTC Synchronous-Reluctance-Motor drives," *IEEE Trans. Power Electron.*, vol. 26, no. 1, pp. 20–28, Jan. 2011.
[11] S. Bolognani, R. Petrella, A. Prearo, and L. Sgarbossa, "Automatic tracking of MTPA trajectory in IPM motor drives based on AC current injection," *IEEE Trans. Ind. Appl.*, vol. 47, no. 1, pp. 105–114, Jan. 2011.
[12] S. Kim, Y.-D. Yoon, S.-K. Sul, and K. Ide, "Maximum torque per ampere (MTPA) control of an IPM machine based on signal injection considering inductance saturation," *IEEE Trans. Power Electron.*, vol. 28, no. 1, pp. 488–497, Jan. 2013.
[13] T. Sun, J. Wang, and X. Chen, "Maximum torque per ampere (MTPA) control for interior permanent magnet synchronous machine drives based on virtual signal injection," *IEEE Trans. Power Electron.*, vol. 30, no. 9, pp. 5036–5045, Sep. 2015.
[14] P. D. C. Perera, F. Blaabjerg, J. K. Pedersen, and P. Thogersen, "A sensorless, stable V/f control method for permanent-magnet synchronous motor drives," *IEEE Trans. Ind. Appl.*, vol. 39, no. 3, pp. 783–791, May 2003.
[15] S.-K. Kim, J.-S. Lee, and K.-B. Lee, "Self-tuning adaptive speed controller for permanent magnet synchronous motor," *IEEE Trans. Power Electron.*, vol. 32, no. 2, pp. 1493–1506, Feb. 2017.
[16] J.-H. Jang, J.-I. Ha, M. Ohto, K. Ide, and S.-K. Sul, "Analysis of permanent-magnet machine for sensorless control based on high-frequency signal injection," *IEEE Trans. Ind. Appl.*, vol. 40, no. 6, pp. 1595–1604, Nov./Dec. 2004.
[17] J.-I. Ha, K. Ide, T. Sawa, and S.-K. Sul, "Sensorless rotor position estimation of an interior permanent-magnet motor from initial states," *IEEE Trans. Ind. Appl.*, vol. 39, no. 3, pp. 761–767, May/Jun. 2003.
[18] B. Han, Y. Shi, X. Song, K. Hong, and K. Mao, "Initial rotor position detection method of SPMSM based on new high frequency voltage injection method," *IEEE Trans. Power Electron.*, vol. 34, no. 4, pp. 3553–3562, Apr. 2019.
[19] B. Sneyers, D. W. Novotny, and T. A. Lipo, "Field weakening in buried permanent magnet AC motor drives," *IEEE Trans. Ind. Appl.*, vol. IA-21, no. 2, pp. 398–407, Mar./Apr 1985.
[20] D. Reigosa, D. Fernandez, T. Tanimoto, T. Kato, and F. Briz, "Comparative analysis of BEMF and pulsating high-frequency current injection methods for PM temperature estimation in PMSMs," *IEEE Trans. Power Electron.*, vol. 32, no. 5, pp. 3691–3699, May 2017.
[21] C. Lai, G. Feng, K. Mukherjee, V. Loukanov, and N. C. Kar, "Torque ripple modeling and minimization for interior PMSM considering magnetic saturation," *IEEE Trans. Power Electron.*, vol. 33, no. 3, pp. 2417–2429, Mar. 2018.
[22] K. Liu and Z. Q. Zhu, "Position offset-based parameter estimation for permanent magnet synchronous machines under variable speed control," *IEEE Trans. Power Electron.*, vol. 30, no. 6, pp. 3438–3446, Jun. 2015.

KIBOK LEE (Member, IEEE) received the B.S. and M.S. degrees in electrical engineering from Korea University, Seoul, South Korea, in 2005 and 2007, respectively, and the Ph.D. degree in electrical engineering from North Carolina State University, Raleigh, NC, USA, in 2016.

From 2007 to 2011, he was a Research Engineer with LG Electronics Research and Development Center, Seoul. From 2016 to 2018, he was a Senior Motor Control Engineer with the General Motors Powertrain Center, Pontiac, MI, USA. He is currently an Assistant Professor with the Department of Mechatronics Engineering, Incheon National University, Incheon, South Korea. His current research interests include motor drives, power conversion systems, and wireless power transfer systems.

YONGSU HAN (Member, IEEE) received the B.S. and Ph.D. degrees in electrical engineering from Seoul National University, Seoul, South Korea, in 2011 and 2017, respectively. From 2017 to 2018, he was a Postdoctoral Researcher with the Department of Electrical and Computer Engineering, Seoul National University. Since 2018, he has been with LG Electronics, Inc., Seoul, as a Specialist Engineer. His research interests include electric machine drives, hybrid/electric vehicles, renewable generation systems, and grid-integrated power systems.